Available online at www.sciencedirect.com

SCIENCE DIRECT®

Earth and Planetary Science Letters 229 (2004) 91–104

EPSL

www.elsevier.com/locate/epsl

Cosmogenic ^{3}He in Himalayan garnets indicating an altitude dependence of the $^{3}He/^{10}Be$ production ratio

E. Gayer[a,*], R. Pik[a], J. Lavé[b], C. France-Lanord[a], D. Bourlès[c], B. Marty[a,d]

[a]*Centre de Recherches Pétrographiques et Géochimiques, CRPG, CNRS-UPR 2300, BP 20, 54 501 Vandoeuvre-Lès-Nancy Cedex, France*
[b]*Laboratoire de Géodynamique des Chaines Alpines, LGCA-UMR 5025, Maison des Géosciences, BP 53, 38041 Grenoble, France*
[c]*CEREGE, UMR 6635 CNRS-Université Aix-Marseille III, BP 80, 13545 Aix-en-Provence Cedex 04, France*
[d]*Ecole Nationale Supérieure de Géologie, ENSG, rue du Doyen Marcel Roubault, BP 40, 54501 Vandoeuvre-Lès-Nancy Cedex, France*

Received 5 May 2004; received in revised form 21 September 2004; accepted 11 October 2004

Editor: K. Farley

Abstract

To investigate the potential of using cosmogenic helium in garnet as a dating tool, $^{3}He_c$ and $^{10}Be_c$ have been measured within garnets and coexisting quartz, respectively, sampled in the Himalayan range at various elevations. Comparison and correlation of $^{3}He_c$ and $^{10}Be_c$ concentrations demonstrate that cosmogenic ^{3}He is well retained in Himalayan garnets and can thus be used in this mineral to quantify precisely earth's surface processes. This, in the case of recently cooled orogenic samples which contain limited amounts of non-cosmogenic helium. For these high-elevation samples, the exposure ages derived from $^{3}He_c$ using classical scaling factors lead however to an overestimation of $^{3}He_c$ ages, compared to $^{10}Be_c$ ages (0.1 to 28 ky), by up to a factor of 2. Additionally, over the samples altitude range (3000–4622 m), the theoretically invariant polar $^{3}He_c/^{10}Be_c$ production ratio (~22.5), increases with increasing elevation, challenging classical models of production rate evolution. To explain this observation, we propose a new $^{3}He_c$ production mechanism, based on the altitudinal dependence of the energy spectrum of cosmic rays, and according to which neutrons or protons resulting from a first spallation reaction within the rock (tertiary particles) may have sufficient energy to induce an additional in situ spallation reaction producing a second ^{3}H or ^{3}He, but insufficient energy to produce ^{10}Be, the probability of such a mechanism increasing with altitude. According to these observations, we propose for future and ongoing studies to use the empirically determined attenuation length of 121 g/cm^2 for helium production at high altitude.

Keywords: ^{3}He; ^{10}Be; production rate; cosmogenic nuclide; garnet; Himalaya; cross-calibration

* Corresponding author. Tel.: +1 617 384 9335; fax: +1 617 496 6958.
E-mail address: egayer@eps.harvard.edu (E. Gayer).

0012-821X/$ - see front matter © 2004 Elsevier B.V. All rights reserved.
doi:10.1016/j.epsl.2004.10.009

1. Introduction

Cosmogenic radionuclides measured in surface rocks are commonly used to determine cosmic ray exposure ages, e.g. [1–3], to date catastrophic events, e.g. [4,5] and to evaluate erosion and incision rates, e.g. [6–8]. Measurements of cosmogenic ^{10}Be (^{10}Be$_c$) and ^{26}Al have been greatly improved in the last decade and are now routinely performed in quartz, e.g. [9–11]. Because they are stable, ^{3}He$_c$ and ^{21}Ne$_c$ allow investigation of extremely long-exposure events [12] compared to other commonly used cosmogenic nuclides [3]. In addition to its low detection limit, ^{3}He$_c$ also has the highest production rate among terrestrial cosmogenic nuclides, e.g. [2,13,14] which makes it particularly well-suited to date recent surfaces and events. However, because of its chemical properties and its small atomic radius, helium diffuses easily at low temperature from many mineral matrices, e.g. [15–18], except from minerals with low ionic porosity such as olivine, pyroxene [2,16], and garnet [19]. Efforts to characterize cosmogenic helium mainly focused on olivines within which the ^{3}He$_c$ production rate was calibrated using independently (^{14}C or ^{40}Ar/^{39}Ar) dated volcanic events, e.g. [13,20–22]. Cosmogenic ^{3}He in olivine then successfully allowed dating geological events and estimating erosion rates, e.g. [23–27]. By contrast, despite its potential when considering metamorphic rocks, cosmogenic ^{3}He in garnet has been neglected due to the presence of a non-cosmogenic component that significantly complicates correction procedures. Indeed, total ^{3}He (^{3}He$_T$) in a mineral represents the sum of inherited ^{3}He (^{3}He$_{in}$, trapped in fluid inclusions and mineral matrix during grain formation), nucleogenic ^{3}He (^{3}He$_n$, produced and retained after grain formation) and cosmogenic ^{3}He (^{3}He$_c$). The nucleogenic component which results from the decay of tritium produced through neutron capture on ^{6}Li (^{6}Li(n,α)^{3}H->^{3}He), is often dominant in Li-rich garnets and therefore may represent the major source of non-cosmogenic ^{3}He.

To investigate the potential of cosmogenic helium in garnet as a dating tool, ^{3}He was measured in garnets sampled in the Himalayan range at various elevations. Our approach represents one of the first attempts to use cosmogenic ^{3}He produced within garnet to date young geological events. To test and calibrate such measurements, ^{10}Be$_c$ was analyzed within the same samples. The two methods have been performed in coexisting garnets and quartz picked from ice-smoothed surfaces and moraines that have recent and simple exposure histories. This study was also designed to intercalibrate cosmogenic nuclide production rates at high elevation (>3000 m), which was previously lacking, and has major implications concerning the validity of scaling factors over the entire atmosphere thickness. This work, for the first time, points out evidence for variations of production rate *ratios* with elevation and suggests that new production mechanisms may occur at high elevation.

2. Geological setting and sampling

The Himalayan range appears to be a particularly well-suited site to investigate ^{3}He$_c$ dating using garnets. The Mio-Pliocene metamorphism experienced by this range resulted in the formation of garnet-rich rocks [28,29], which cooled only a few My ago [30] which minimizes the accumulation of ^{3}He$_n$. This study focused on geomorphic features associated with the last Holocene glacier retreat that thus have simple exposure histories. Most of the samples were collected at elevations ranging from 3510 to 4622 m from blocks on top of recessional moraines as well as from ice-smoothed striated surfaces sampled in the upper part of the Mailun Khola river in the Ganesh Himal (85.18°E, 28.23°N, Fig. 1). Rocks from this area, which are mostly high-grade metamorphic schists, belong to the Main Central Thrust (MCT) zone where the High Himalayan Crystalline (HHC) formation is underlined by the Lesser Himalayan (LH) formations [29,31]. Coexisting quartz has been extracted from the sample gangues (Table 1).

In order to test the rock depth dependence of ^{3}He$_c$ and ^{10}Be$_c$ productions, three samples were taken (Table 1) along a 90-cm-long profile recently exhumed near the entry of a mine, located at an elevation of 4125 m in the Mailun Khola valley (Fig. 1). The original depth has been reconstructed from the apparent shape of the remaining 26°-dipping surface, and is therefore subject to a rather large uncertainty. Some shielded rocks were also sampled in the mine in order to check the validity of non-cosmogenic component corrections (Table 1, Fig. 1). Five samples were taken along the gallery, corresponding to

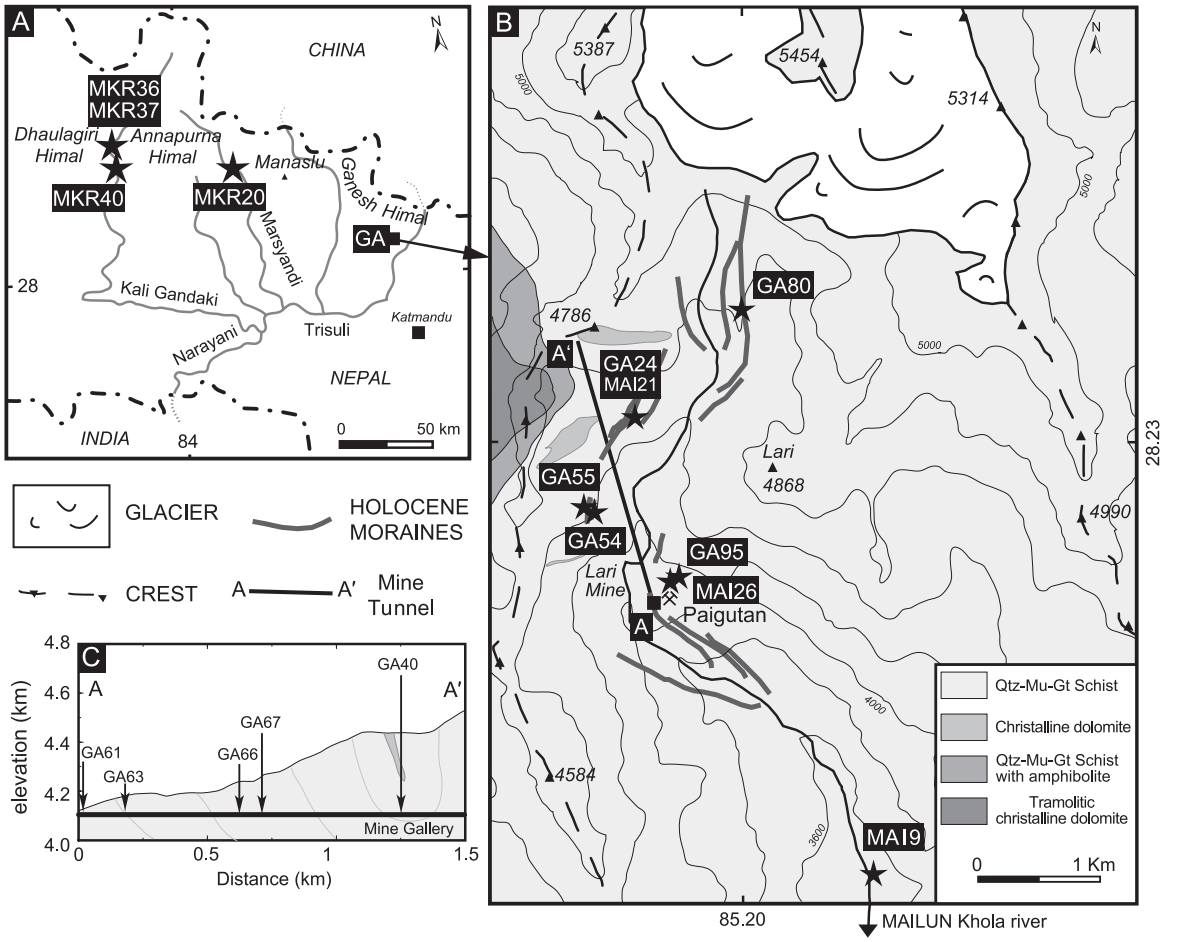

Fig. 1. (A) Location of sampled sites in Central Nepal. (B) Geological map of the upper Mailun Khola river indicating the location of sampling areas along the glacier retreat path from MAI9 to GA80, as well as the main Holocene moraines. The Lari mine from where shielded rocks have been sampled is located near Paigutan. (C) Topographic profile along the mine gallery (A-A′) indicating the position of the various shielded samples.

shielding by rock thicknesses ranging from ~10 to ~300 m.

To extend the altitudinal range, a biotite-rich gneiss (MKR20) was sampled in the Manaslu Himal, on a lateral abrasion surface of the Marsyandi river canyon (84.36°E, 28.50°N) at an elevation of 1950 m, and two garnet-rich orthogneisses (MKR36 and MKR37) were sampled in the Annapurna Himal, on a terrace in the Kali Gandaki valley (83.62°E, 28.66°N) at an elevation of 3000 m (Fig. 1). A boulder from the top of an old mid-Holocene debris flow was also sampled at an elevation of 1700 m (MKR 40) (Fig. 1). For all the samples but the Marsyandi one, topographic masks were low (mask correction factors between 0.95 and 1).

3. Analytical methods

After rock crushing, all grains were extracted from fractions sieved between 0.315 and 0.500 mm. Subsequent separation was performed using standard heavy liquid techniques, as well as additional magnetic treatment when necessary. Final separation and cleaning have been done by hand-picking under a binocular microscope.

Table 1
$^{3}He_c$ and $^{10}Be_c$ concentrations and sample characteristics

Samples	Sampling			Outcrop	Quartz	Weight (g)	$^{10}Be_c$ (10^4 at/g)	Garnet	Weight (mg)	$^{4}He_T$ (10^{13} at/g)	$^{3}He_T$ Blk corr. (10^6 at/g)	$^{3}He_c$ (10^6 at/g)	Li (ppm)
	Lat. (°)	Alt. (m)	Depth (m)										
Exposed surfaces													
GA24	28.23	4490	0	M	RO	32.3	31.78±3.31	SG	10.3	7.50±0.38	20.57±1.14	17.17±1.29	32±4
									10.3	10.70±0.55	20.03±1.45		
GA54	28.23	4434	0	M	RO	33.7	31.73±3.22	SG	9.4	3.89±0.22	16.79±0.91	14.65±1.36	43±7
						15.1	39.75±3.76		10.2	7.37±0.38	18.24±1.45		
GA55	28.23	4446	0	M	RO	6.6	58.78±6.89	SG	10.4	4.20±0.22	23.13±1.32	21.11±6.83	39±2
										2.67±0.14	31.34±1.42		
										4.06±0.21	15.84±1.45		
GA80	28.24	4622	0	M	RO	10.5	0.83±0.80	RO	7.7	7.82±0.40	3.46±1.14	0.48±0.56	24±3
						22.3	0.80±0.80		10.1	2.98±0.15	1.61±0.32		
									11.1	4.59±0.24	2.12±0.76		
MKR20	28.50	1950	0	S	RO	20.1	2.64±0.95	RO	10.5	3.92±0.20	0.90±0.51	0	20±5
						6.4	1.91±1.74		10.5	6.35±0.33	1.21±0.74		
									10.8	4.24±0.22	2.69±0.36		
MKR36	28.66	3000	0	T	RO	17.8	70.63±17.78	RO	10.9	10.94±0.56	33.41±1.24	23.52±3.83	105±20
						7.1	62.07±6.85		10.8	14.90±0.76	30.31±1.59		
GA95	28.22	4150	0	PS	RO	12.3	38.53±3.72	SG	10.3	1.49±0.08	13.92±0.83	12.92±0.85	40±7
									10.2	1.90±0.10	14.95±1.40		
									11.0	1.14±0.58	15.02±1.58		
									10.0	6.15±0.32	16.84±1.14		
MKR40	28.58	1700	0	T	RO	11.4	3.94±1.09	RO	10.9	67.90±3.40	17.86±1.45	5.54±2.54	6±1
									9.8	42.82±2.15	11.84±1.20		
									9.7	62.84±3.15	20.40±0.99		
									10.7	63.81±3.19	21.64±1.13		
MKR37	28.66	3000	0	T	RO	11.7	85.94±6.72	RO	10.7	26.09±1.31	28.33±0.54	18.59±2.55	94±6
									11.0	10.64±0.53	24.84±1.25		
									10.5	13.79±0.69	25.92±1.20		
MAI9	28.21	3510	0	PS	RO	13.9	36.13±3.33	SG	9.6	0.44±0.05	11.84±1.07	11.84±0.93	30±1
									9.6	1.09±0.06	13.33±0.71		
Depth profile													
MAI26	28.22	4125	0	PS	RO	9.9	30.33±3.65	SG	10.4	7.51±0.38	16.41±1.18	14.10±1.34	58±12
									10.2	5.42±0.27	18.82±1.30		
									10.0	5.49±0.28	17.40±1.12		
MAI25	28.22	4125	0.42	BS	RO	4.3	13.76±3.87	SG	10.0	2.09±0.12	8.87±1.08	8.37±1.25	–
									9.6	2.15±0.11	10.99±0.90		
MAI24	28.22	4125	0.73	BS	RO	11.7	12.14±2.63	SG	10.5	1.70±0.09	4.68±0.78	4.39±0.88	40±1
									10.6	3.46±0.18	7.87±0.68		
									10.5	2.74±0.14	6.61±0.57		
Mine samples													
GA40	28.23	4100	307	MS	–	–	–	RO	9.9	4.61±0.24	0.63±0.52	0	23±2
									10.1	5.74±0.30	0.82±0.73		
GA66	28.23	4100	210	MS	–	–	–	RO	11.4	7.41±0.38	2.60±0.48	0	32±3
									10.6	7.28±0.37	2.77±0.44		
GA67	28.23	4100	220	MS	–	–	–	RO	10.6	7.95±0.41	1.37±0.98	0	43±5
									11.7	11.27±0.58	2.32±0.97		
GA61	28.22	4100	≈10	MS	–	–	–	RO	10.5	7.95±0.41	2.10±0.96	0	42±5
GA63	28.22	4100	50	MS	–	–	–	RO	10.5	1.89±0.01	0.90±0.92	0.18±0.86	17±2

3.1. ^{10}Be measurements

To avoid potential contamination by meteoric ^{10}Be, quartz was first purified by dissolving other minerals in a HNO_3–H_2SiF_6 mixture [32,33]. Although this procedure is supposed to readily eliminate most part of surface meteoric contamination, the decontamination procedure is pursued further by dissolving through three cleaning steps in HF about 30% of the obtained quartz fraction. The quartz fraction remaining after these ultimate decontamination steps was then totally dissolved in HF. After addition of a ^{9}Be spike [33], beryllium was purified by solvent extraction and precipitation [32–35]. $^{10}Be_c$ concentrations were measured at the Tandetron Accelerator Mass Spectrometry Facility, Gif-sur-Yvette, France. ^{10}Be uncertainties, reported as 1σ, were calculated by propagating a conservative estimate of 5% instrumental uncertainty, as well as the uncertainties associated with counting statistics and blank correction [36].

3.2. ^{3}He measurements

About 10 mg of garnet grains was handpicked and ultrasonically cleaned in acetone at room temperature for 10 min. Helium was extracted from such aliquots by vacuum melting using a CO_2 laser [37,38]. The evolved gas was cleaned over a hot Ti-getter and a charcoal trap held at liquid nitrogen temperature [38–40]. Helium was then separated from Ne at 15 K and analyzed for abundance and isotope composition using the Static Mass Spectrometer (VG 5400) of CRPG, Nancy, France.

Because this study revealed apparent inconsistencies between $^{3}He_c$ and $^{10}Be_c$ ages, the ^{3}He measurements were carefully checked: (i) two different He standards were used for calibration, (ii) two different analytical lines were used in CRPG, which had been previously cross-calibrated at better than 3% (using Durango apatite standard grains and helium-doped glass spherules) and, (iii) a cross-calibration was done with the ETH noble gas laboratory (Zurich, Switzerland) on the GA98 sample (Table A1 available as a Background Data Set). All of the intercalibration checks agree within a few percent for the ^{3}He concentration measurement and do not reveal any particular calibration offset between the two labs or between the two CRPG extraction systems.

Typical ^{3}He and ^{4}He blanks were $9.03–9.64\times10^{3}$ and $3.01–3.61\times10^{9}$ atoms, respectively. For ^{3}He, the precision of individual measured concentrations is 10% or better for most of the samples, but can be as poor as 30–50% for the youngest samples (<1 ky, GA80, MKR20, and the shielded mine samples, Table 1), which contain very low amounts of ^{3}He ($<3.5\times10^{6}$ at/g).

Special care was taken to handpick, under a binocular, garnet grains free of visible inclusion to minimize the $^{3}He_n$ contamination by Li-rich minerals. However, due to their spiral characteristics, it was not possible to extract 10 mg of material free of any inclusions for all the samples. Electron microprobe analysis showed that most of the observed inclusions in these garnets are ilmenites. To test if the ilmenites are the source of nucleogenic helium, the ^{3}He content has been measured in 15 variously "contaminated" aliquots of the same garnet sample (Table A1 available as a Background Data Set). The results are remarkably homogeneous and do not show any correlation of ^{3}He with the density of impurities, even for the aliquot with the highest ilmenite contamination. Notably, the standard deviation of the duplicates, 11.9% (1σ), is similar to the uncertainty of an individual measurement, strongly suggesting that the main source of uncertainty is analytical rather than natural in the case of this sample.

4. Results

4.1. ^{10}Be results

The Marsyandi and Kali Gandaki samples, collected at intermediate elevation, yield $^{10}Be_c$ concen-

Notes to Table 1:
M: moraine, S: abrasion surface, PS: ice-smoothed surface, T: terrace boulder, BS: buried sample, SG: single garnet, MS: mine sample, RO: quartz and garnets from whole rock, in this case the sample size does not exceed an average of 1.5 cm and does not necessitate shielding correction. ^{10}Be blank concentrations range from 1.04×10^{5} to 2.12×10^{5} at/g. Typical ^{3}He blank concentrations range from 9.03 to 9.64×10^{3} atoms. Li concentrations in garnets have been measured on single garnet grains from different aliquot by ion probe (Cameca IMS 3F, CRPG).

trations ranging from 1.91×10^4 to 85.94×10^4 at/g (Table 1). In the higher Mailun Khola glacial valley, the measured concentrations, which range from 0.80×10^4 to 58.78×10^4 at/g, are consistent with the relative chronology of the sampled moraines, estimated from geomorphic criteria.

4.2. ^{3}He results

A global estimate of the non-cosmogenic ^{3}He is given by the He data measured in the shielded samples from the mine ($<3.3\times10^6$ at/g taking account of the error limits, black dots in Fig. 2). Except for samples younger than 1 ky (GA80 and MKR20, open dots in Fig. 2B), the amounts measured within the shielded samples are significantly lower than the concentrations measured within samples from exposed surfaces and moraines (Fig. 2A). This indicates that ^3He_c can be discriminated in the collected Himalayan samples.

More precisely, ^3He_c concentrations can be derived from the measured ^3He_T concentrations by subtracting the non-cosmogenic components, which are: (i) a potential inherited component (e.g., $^3He_{in}$ from crustal fluids incorporated during garnet formation), and (ii) the nucleogenic helium (^3He_n, produced and retained after cooling of the garnets).

$$^3He_c = {}^3He_T - ({}^3He_{in} + {}^3He_n) \quad (1)$$

^3He_n is produced from beta decay of ^{3}H, itself produced by thermal neutron irradiation on ^{6}Li and low energy α-particle on ^{11}B, the latter mechanism being generally negligible. The full developed equation for cosmogenic ^{3}He calculation for an aliquot i writes:

$$^3He_c^i = {}^3He_T^i - \left(\frac{^3He}{^4He}\right)_{in}\left(^4He_T^i - P_{^4He_{rad}\left(U_G^i,Th_G^i\right)}t_i\right) - P_{^3He_n\left(U_R,Th_R,X_R,Li_G^i\right)}t_i \quad (2)$$

where $P_{^3He_n}$ is the nucleogenic ^{3}He production rate, proportional to:

(i) the elapsed time since closure of the garnet phenocrysts to helium diffusion,

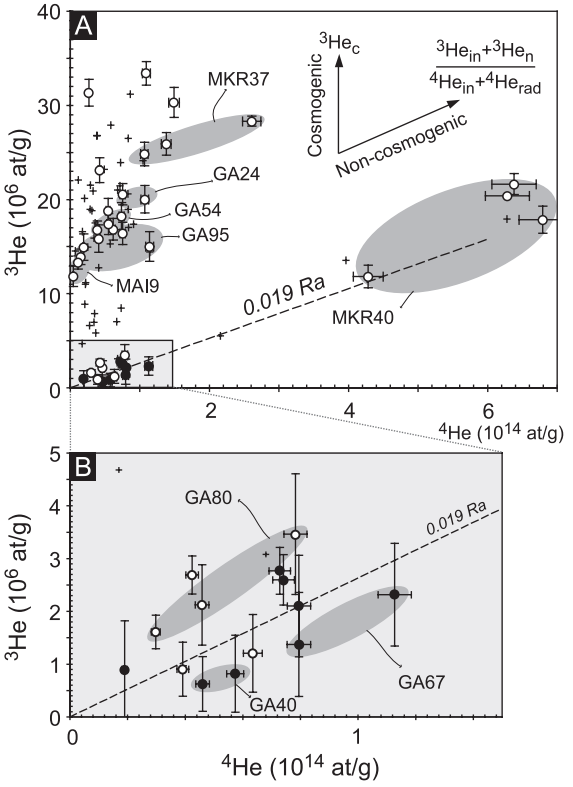

Fig. 2. ^{3}He vs. ^{4}He concentrations of garnets measured in this study. Exposed garnets are indicated by open symbols while the shielded mine samples are indicated by black symbols. Black crosses correspond to all the other garnets measured in the more general framework of a companion study dedicated to the Mailun Khola glacier Holocene retreat [57], and for which ^{10}Be analyses are not available. The ellipse-shaped fields indicate the analysis of the various aliquots of the same sample for which the number is also indicated. The correlation, with an isotopic ratio of 0.019 Ra±0.014, represents the crustal inherited component (Marty and France-Lanord, unpublished data). The indicated end-member components are: ^3He_c: cosmogenic helium, $^3He_{in}$, $^4He_{in}$: trapped inherited crustal helium, ^3He_n: nucleogenic helium, $^4He_{rad}$: radiogenic helium.

(ii) the local neutron flux, which depends on the U and Th composition (U_R,Th_R) of the surrounding host rock within a distance of ~1 m.

(iii) the fraction of thermal neutrons absorbed in the garnet crystal (Li_G), which depends on its composition (Li, B) and on the abundance of all the elements present in the host rock (X_R=Fe, Gd, Si, K, Al, Ti … and other major and traces elements in order of their contribution to neutron absorption [41]).

The radiogenic production rate ($P_{4_{He_{rad}}}$) can be calculated from the U and Th content of the mineral (U_G,Th_G) [42].

In the case that there is no inherited component, the equation can be simplified in:

$$^3He_c^i = {}^3He_T^i - {}^4He_T^i\left(\frac{P_{3_{He_n}\left(U_R,Th_R,X_R,Li_G^i\right)}}{P_{4_{He_{rad}}\left(U_G^i,Th_G^i\right)}}\right) \quad (3)$$

Determination of the cosmogenic component requires therefore multiple information, i.e. the time of closure to helium diffusion, the chemical composition of the host rock and determination of ^{3}He, ^{4}He, Li, U and Th concentrations in the same garnet aliquot.

The analytical procedure followed for garnets, in particular the garnet laser fusion to measure helium isotopes with very low blank levels, prevents measurement of all these elements in the same aliquot. Moreover, because U and Th measurements in garnets require a Li-metaborate fusion before dissolution [43], measurements of ^{3}He+^{4}He, Li, and U+Th had to be conducted on different aliquots. This procedure is valid as long as concentrations in Li, U and Th are relatively homogeneous in all the garnets of a given sample. This is fairly true for the Li, which is mostly contained in the phenocrysts matrix of the analyzed garnets. In contrast, U and Th measurements display a larger heterogeneity in the same sample (Fig. 3A, Table A2 available as a Background Data Set). As suggested by in situ ion microprobe analysis (Cameca IMS 3F, CRPG), this feature is probably linked to the absence of these elements in the matrix of the garnets, and their possible presence in U–Th-rich inclusions like monazite and zircon. In spite of this large concentration variability, the U and Th composition of garnets co-vary and there is an equal partitioning coefficient for these two elements since the host rocks align on the same trend (Fig. 3A).

For the different aliquots of the same sample, the variations in U and Th-rich inclusions might induce large $^4He_{rad}$ variations (Fig. 3B) since ^{3}He is supposed to stay more or less constant. However, numerous samples, as observed in Fig. 2, display a clear trend between ^{3}He and ^{4}He. This slope is compatible with the crustal inherited isotopic ratio as deduced from the Nepalese hot springs composition (0.019 Ra, Marty and France-Lanord, unpublished data), and could be

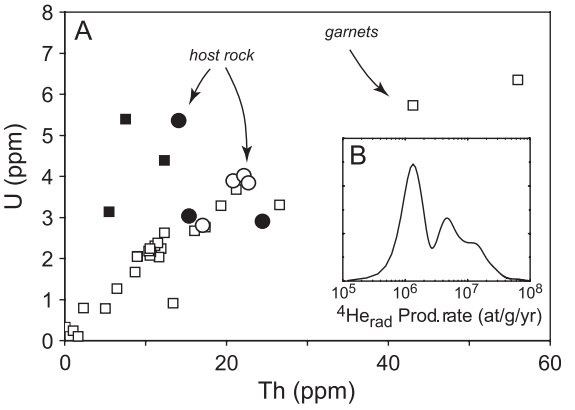

Fig. 3. (A) U and Th concentrations measured in the garnets and host rocks of this study by ICP-MS Elan 6000 following Carignan et al. [43] (Table A2 available as a Background Data Set). Open symbols correspond to the Mailun Khola valley samples, whereas filled symbols correspond to the Marsyandi and Kali Gandaki valley samples. (B) Density probability of radiogenic ^{4}He production rate in the garnets calculated following Eq. (2) (see text available as a Background Data Set).

explained by variations in the number and volume of fluid inclusions. Alternatively, these trends could be interpreted as a mixing, if the different parts of the garnets have degassed their radiogenic and nucleogenic helium in a heterogeneous manner. As a consequence of these [^{4}He] variations, the specific (U–Th)/He ages performed on garnets from the mine samples, to evaluate their thermochronological history, are very heterogeneous (Table A3 available as a Background Data Set). However, the average of the garnet (U–Th)/He ages is close to 3–4 My, which ranges between the Ar-age in muscovite (Lavé, unpublished data) and the He-age in apatite (Table A3 available as a Background Data Set), and which suggest an intermediate closure temperature for helium in garnets.

The analytical procedures and the large unknowns in helium diffusion and degassing, results in under determination of Eq. (2). Therefore, we have adopted a general Monte Carlo probabilistic approach to compute cosmogenic ^{3}He by assuming that a crustal inherited component is preserved in garnets (see text available as a Background Data Set). This correction procedure has been proven to be valid with the shielded mine samples: The results of the two correction models, Eqs. (2) and (3) (with and without crustal helium), give very similar calculated concentrations that account for the measured values

within error (Fig. 4). The slight difference between modeled and measured non-cosmogenic concentrations on shielded samples corresponds to a ^{3}He concentration equivalent to less than 1 ky exposure at this altitude. Moreover, as shown for most of the shielded samples (Fig. 4), the parameterization of our model tends to overestimate, rather than underestimate, the non-cosmogenic component, which indicates that derived cosmogenic concentrations would not be affected by incomplete correction. Note that the applied correction is appropriate for these garnets because their very recent cooling (<10 My) accumulates of a very limited amount of nucleogenic ^{3}He.

4.3. Cosmogenic concentrations

The corrected $^{3}He_c$ concentrations, which range from 0.48×10^{6} to 23.52×10^{6} at/g (Table 1), as well as the associated $^{10}Be_c$ concentrations are in agreement with the relative chronology of the glacial features sampled in the Mailun Khola valley. As expected, the lowest concentrations are related to moraines closest to the present-day glacial tongue. More importantly, the observation that the $^{3}He_c$ vs. $^{10}Be_c$ plot goes through the origin (Fig. 5) indicates that the corrections applied to $^{3}He_T$ are reasonable, and that the derived $^{3}He_c$ concentrations do not suffer from

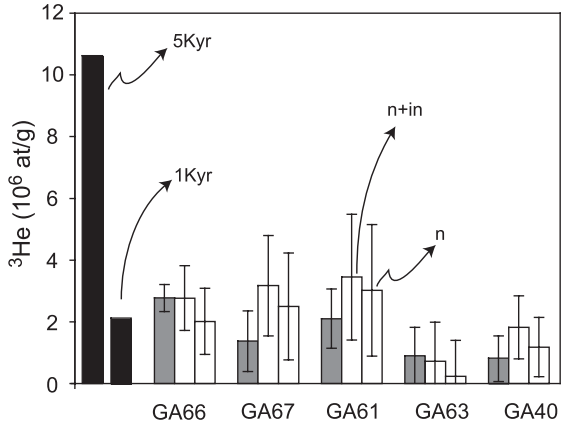

Fig. 4. Comparison of measured and calculated ^{3}He concentrations in the garnets from the mine-shielded samples. Grey sticks correspond to the ^{3}He measured concentrations. White sticks correspond to the ^{3}He concentrations calculated following Eqs. (2) and (3), respectively (n+in and n). The calculated concentrations are in good agreement with the measured values, within errors. For comparison, the black sticks correspond to the ^{3}He concentrations produced for exposure time of 1 and 5 ky (at the mine altitude).

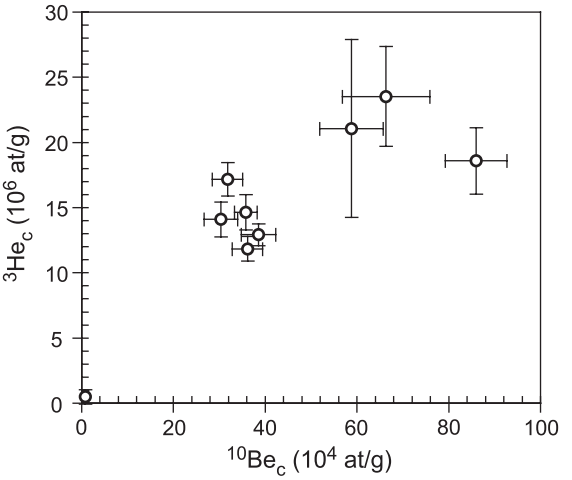

Fig. 5. $^{3}He_c$ vs. $^{10}Be_c$ concentrations showing correlation from high to very low concentrations.

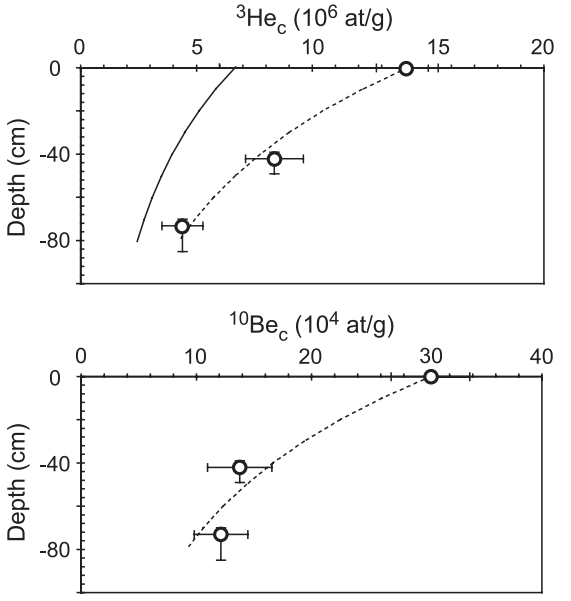

Fig. 6. Depth profile for $^{3}He_c$ and $^{10}Be_c$ concentrations. The dashed line represents the calculated decrease of each cosmogenic nuclide with depth, starting from the measured surface concentration, for an attenuation length of 180 g/cm^{2} and a rock density of 2.71 g/cm^{3}. The black line in the ^{3}He depth profile figure represents, for comparison, the same calculated profile but starting from the ^{3}He concentration calculated from the expected production rate of Dunai [49] and the ^{10}Be exposure age using same attenuation parameters.

significant and systematic incomplete subtraction of the nucleogenic and/or inherited component. The cosmogenic nature of the ^{3}He corrected concentrations is also strongly supported by the exponential decrease of these concentrations with the expected attenuation length over the 90-cm-thick depth profile, as presented in Fig. 6.

5. Discussion

5.1. Exposure age calculations

In order to determine cosmic ray exposure ages from the $^{10}Be_c$ concentrations measured in quartz, a $^{10}Be_c$ production rate of 5.1±0.3 at/g/year at sea level and high latitude was used [44]. Assumed negligible losses due to erosion are justified by the expected short exposure duration of the studied samples. Since the production rate for $^{3}He_c$ in garnet has never been published, the production rate of $^{3}He_c$ in olivine of 115±4 at/g/year at sea level and high latitude [14,20–22,45] was used, considering, as suggested by models [46,47], a limited compositional dependence. These sea level and high latitude production rates have been scaled for the sampling latitudes and altitudes using the scaling factors proposed by Lal [48] and Dunai [49], with corresponding errors of 2% at sea level, 6% at 3000 m, and 10% at 5000 m (Table 2).

For both cosmogenic nuclides, the $^{3}He_c$ and $^{10}Be_c$ exposure ages calculated using the Lal [48] and Dunai [49] scaling factors are very similar within errors (Table 2). The $^{10}Be_c$ exposure ages range from 0.1 to 28 ky, while the corresponding $^{3}He_c$ derived exposure ages range from 0.2 to 34 ky (Table 2). For each sample, the exposure age calculated from $^{3}He_c$ within garnet appears to be systematically two times higher than the exposure age calculated from $^{10}Be_c$ in quartz (Fig. 7). Such a systematic discrepancy could be due either to an incorrect estimation of cosmogenic ^{3}He or ^{10}Be concentrations, or to the use of an inappropriate production rate. As demonstrated in the previous section, overestimation of the $^{3}He_c$ concentrations cannot be related to incomplete subtraction of inherited helium. The concentration offset may instead be linked to analytical biases. Since a careful check of the analytical procedures for both cosmogenic nuclides, and an intercalibration with the ETH noble gas laboratory (Kober and Wieler, unpublished

Table 2
Comparison of $^{3}He_c$ and $^{10}Be_c$ exposure ages

Sample	Alt. (m)	^{10}Be (Lal, 1991)	^{10}Be (Dunai, 2000)	^{3}He (Lal, 1991)	^{3}He (Dunai, 2000)	^{3}He (this study)	
			Λ=145 g/cm^2		Λ=145 g/cm^2	Λ=121 g/cm^2	
		Exposure age (year)	Exposure age (year)	Exposure age (year)	Exposure age (year)	Prod. rate (at/g/year)	Exposure age (year)
GA24	4490	4341±679	4359±682	10404±1357	10447±1363	2915±292	5890±737
GA54	4434	5043±687	5080±692	9165±1300	9231±1310	2797±280	5236±715
GA55	4446	8301±1382	8356±1391	13193±4506	13280±4536	2801±280	7522±2551
GA80	4622	105±83	104±83	275±324	275±323	3160±316	153±179
MKR36	3000	20174±3374	21593±3611	31710±5631	33940±6027	1022±102	23007±4397
GA95	4150	6372±979	6512±1000	9478±1206	9685±1232	2280±228	5667±677
MKR37	3000	26132±3032	27969±3246	25068±3864	26831±4136	1022±102	18188±3084
MAI9	3510	10276±1446	10821±1522	14942±1762	15735±1855	1195±120	9910±1262
MAI26	4125	5230±901	5351±921	10785±1585	11036±1622	2178±218	6474±892
GA24*	4490	4897±766	4917±769	11736±1531	11784±1537	2584±258	6644±832
		^{14}C Age					
MAI21		6100±100					

^{14}C results provided by Center for accelerator mass spectrometry; Lawrence Livermore National Laboratory. Exposure ages calculated using published scaling procedures of Dunai [49], scaling procedures of Lal [48] and using the attenuation length (Λ=121 g/cm^2) proposed in this study.

* Snow cover corrected.

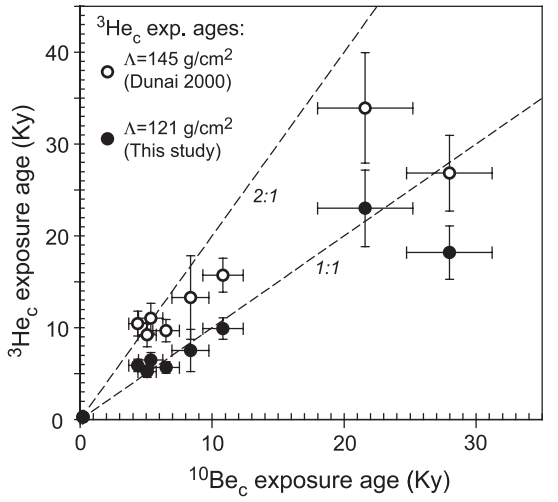

Fig. 7. ^{3}He$_c$ ages vs. ^{10}Be$_c$ ages. Open circles correspond to ^{3}He$_c$ ages and ^{10}Be$_c$ ages calculated with Dunai's scaling factor [49] (Table 2). Black circles correspond to ^{3}He$_c$ ages calculated from the ^{3}He production rate model of this study (Λ=121 g/cm^2) vs. ^{10}Be$_c$ ages calculated with Dunai's scaling factor [49] (Table 2).

data, Table A1 available as a Background Data Set), do not reveal any biases, the observed age discrepancy is most likely related to the values of production rate used in the calculations.

In order to determine which production rate is incorrect, the age of the glacier retreat was independently estimated through the ^{14}C dating of an organic matter-rich level buried at a depth of 1.5 m in a small lake developed behind a moraine (MAI21 Fig. 1). The obtained ^{14}C age of 6.1±0.1 ky (MAI21, Table 2) agrees with the snow cover corrected 4.9±0.8 ky ^{10}Be$_c$ age determined for the summit boulder of the moraine (GA24*, Table 2), but is discordant with the snow cover corrected 11.8±1.5 ky ^{3}He$_c$ age obtained for the same boulder (GA 24*, Table 2). It therefore appears that this age discrepancy is most likely related to the ^{3}He$_c$ production rate.

5.2. Compositional and altitudinal dependences of ^{3}He$_c$ production rate

Even if the garnet matrix contains different targets, e.g. Al and Ca, for ^{3}He$_c$ production than that of olivine, theoretical calculations of ^{3}He production rates at sea level and high latitude [46,47] for spallation from galactic cosmic ray particles on major elements (O, Si, Al, Mg, Ca, Fe) do not suggest significant ^{3}He$_c$ production variations (<20%) in these two minerals. Moreover, recently published data [22] do not highlight important production differences between pyroxene and olivine, which present strongly contrasted compositions for Ca and Al.

In addition to the higher than expected ^{3}He$_c$ production rate in garnets, a general tendency for a higher ^{3}He$_c$/^{10}Be$_c$ ratio with increasing altitude is suggested by the data (Fig. 8). Theoretically, the ^{3}He$_c$/^{10}Be$_c$ production ratio should remain constant with altitude (~22.5), since the scaling procedure is identical for both cosmogenic nuclides [48,49]. However, as presented in Fig. 8, there is an altitudinal dependence of the ^{3}He$_c$/^{10}Be$_c$ ratio, which is clearly resolved from the theoretical production ratio [21,48]. The trend displayed in Fig. 8 suggests that the observed excess ^{3}He$_c$ is reduced at low altitudes, where ^{3}He$_c$/^{10}Be$_c$ (~22.5), corresponds to the previously determined production values for both isotopes

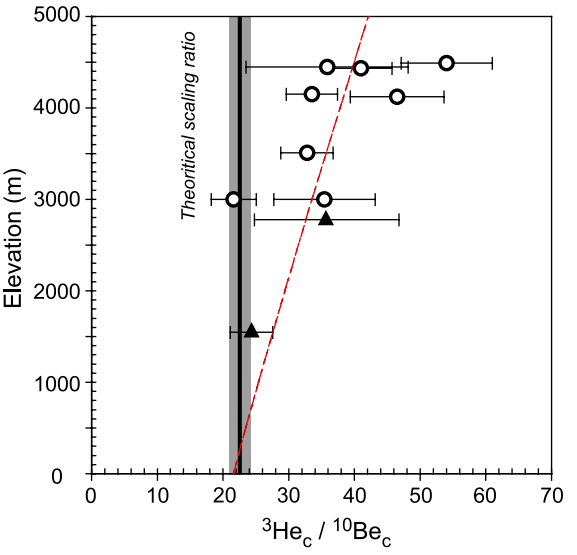

Fig. 8. Elevation against ^{3}He$_c$/^{10}Be$_c$ ratio. Open circles correspond to the garnet samples of this study, and the triangles to samples from previous studies (Licciardi et al. [25] and Nishiizumi et al. [52]). The theoretical value of ~22.5 corresponds to the polar production rate ratio [48,49] which is conservative through classical altitudinal scaling procedures. Our data do not fit this theoretical value with altitude, suggesting different altitudinal dependence for ^{3}He$_c$. The dashed line represents the altitudinal variation of ^{3}He$_c$ and ^{10}Be$_c$ production calculated, respectively, with Λ of 121 and 145 g/cm^2.

[4,13,14,50,51]. This tendency is supported by two other studies (black triangles in Fig. 8) that also measured cosmogenic ^{3}He and ^{10}Be concentrations within olivine and quartz from the same samples, respectively [25,52].

Even if the observed altitudinal dependence of the $^{3}He_{c}$ production rate probably corresponds to a different function than the one used by Dunai [49], the apparent attenuation length fitting all the data included in Fig. 8, using this published scaling procedure, corresponds to 121 g/cm^{2}, which is lower than the one commonly used (about 145 g/cm^{2} at this latitude [49]).

5.3. Potential mechanisms for high elevation cosmogenic ^{3}He excess production

In order to account for the observed increase in $^{3}He_{c}$ production relative to $^{10}Be_{c}$ with increasing elevation, at least two different processes may be invoked. We may first think of the combined action of the secondary particles already included in low altitude models (i.e. cosmic ray secondaries inducing spallation reactions: Λ=145 g/cm^{2}) but with additional particles specific to high elevations. In this case, these hypothetical high elevation "efficient particles" would have to be characterized by an atmospheric attenuation length (Λ) <90 g/cm^{2} (using Dunai's altitudinal function [49]) in order to satisfy the observed apparent attenuation length of 121 g/cm^{2}.

On the other hand, the increase of the $^{3}He_{c}/^{10}Be_{c}$ production ratio with altitude may result from significantly different energy thresholds for ^{3}H, ^{3}He and for ^{10}Be production from the cosmic ray secondaries already considered. Published energy thresholds [53,54] for various target isotopes and projectiles indeed suggest energy thresholds for the production of ^{3}H and ^{3}He at least three to four times lower than those necessary for the production of ^{10}Be. In addition, since, according to Lal and Peters [55], the energy spectrum of cosmic rays >500 MeV is altitude-dependent, the observed altitude dependence of the $^{3}He_{c}/^{10}Be_{c}$ production ratio could be tentatively attributed to cosmic particles having an energy >500 MeV whose contribution increases with altitude. Such >500 MeV energy particles could produce neutrons or protons from the initial spallation reaction within the rock (tertiary particles) that may have an energy high enough to induce a supplementary in situ spallation reaction producing a second ^{3}H or ^{3}He. These particles would not be sufficiently energetic to produce ^{10}Be. The probability of such a mechanism would increase with altitude. This mechanism would imply that cosmogenic ^{3}He and ^{10}Be are both produced primarily through spallation reactions, but that their specific production rates depend on the fluence of incident particles that varies with altitude.

Although the depth profiles presented in Fig. 6 have to be considered cautiously, the resulting ^{3}He attenuation length of 180±10 g/cm^{2} is in agreement with previously published values [51]. This suggests that the "overproduction" of $^{3}He_{c}$ observed at the surface continues at depth. Therefore production of $^{3}He_{c}$ from low attenuation length particles (Λ<90 g/cm^{2}) that would be efficiently attenuated within a few centimeters of rock should be negligible and cannot sustain the observed $^{3}He_{c}$ concentrations at depths greater than 80 cm (Fig. 6). This thus favors the hypothesis of an energy-dependent mechanism to explain the observed altitudinal $^{3}He_{c}$ production rate evolution.

The observations and processes discussed above are not in agreement with $^{3}He_{c}$ production rates measured in exposed water tanks at high elevation in the Mont Blanc massif (France) [56]. However, as ^{3}He production is limited to oxygen, the processes involved in that experiment are not necessarily relevant for more complex and denser matrices such as silicates. Additionally, because of the use of a strongly tritiogenic initial water in the Brown et al. [56] study, the $^{3}He_{c}$ production from ^{3}H decay was not precisely measured.

The results presented here suggest that the energy dependence of cosmogenic ^{3}He production mechanisms is different from that classically considered in the usual scaling procedures. This observation has important implications for the use of $^{3}He_{c}$ at intermediate and high altitudes, and therefore needs to be confirmed by other studies combining cosmogenic isotopes. Beside a more complete database of cosmogenic production rates over a wide range of altitudes, the cosmogenic nuclide energy-dependent production mechanisms must be physically better understood to be correctly incorporated into numerical models of production.

6. Conclusion

This study investigated the possible use of cosmogenic helium in garnet for quantifying earth's surface processes, as well as the helium and beryllium production rate intercalibration. We draw the following conclusions:

(1) Comparison and correlation of the $^{3}He_c$ and $^{10}Be_c$ concentrations, respectively, measured within garnet and quartz coexisting in the samples, has demonstrated that $^{3}He_c$ is well retained in garnet, and can thus be used to quantify earth's surface processes in recently cooled rocks such as in the Himalayan range.

(2) Comparison of the $^{3}He_c$ and $^{10}Be_c$ concentrations, and deduced exposure ages (0.1 to 28 ky), within garnet and coexisting quartz at high elevation has, however, also revealed that the $^{3}He_c/^{10}Be_c$ production ratio increases with increasing elevation, challenging the classical models of production rate evolution.

(3) Consequently, the apparent atmospheric attenuation length for $^{3}He_c$ that fits the obtained data between 3000 and 5000 m (using the Dunai's altitudinal function) correspond to 121 g/cm^2 at the latitude of the studied site (28.5°N). However, the observed altitudinal dependence of the $^{3}He_c$ production rate probably corresponds to a more complex function than the one used here, and needs to be investigated by physical and other experimental approaches.

(4) Rather than the involvement of hypothetical low-attenuation length particles to account for this $^{3}He_c/^{10}Be_c$ altitudinal dependence, we propose, based on the altitudinal dependence of the energy spectrum of cosmic rays, that neutrons or protons resulting from a first spallation reaction within the rock (tertiary particles) may have sufficient energy to induce a supplementary in situ spallation reaction producing a second ^{3}H or ^{3}He, but not high enough to produce ^{10}Be. The probability of such a mechanism increasing with the altitude.

(5) Until future investigations clarify the mechanisms involved in in situ production of $^{3}He_c$, we propose that the empirically determined attenuation length of 121 g/cm^2 is used for production of cosmogenic helium at high altitude (>3000 m).

Acknowledgements

This research was funded by the Institut National des Sciences de l'Univers (INSU-CNRS) through the PROSE and PNSE programs. We wish to thank L. Zimmermann for his assistance in the CRPG noble gas laboratory, R. Braucher for his assistance in the CEREGE ^{10}Be laboratory, and Eric Lewin for discussions concerning Monte Carlo and statistics procedures. We would like to extend particular thanks to F. Kober and R. Wieler for participating in the framework of this study to a first ETH and CRPG noble gas laboratories intercalibration. The comments of R. Wieler, N. Arnaud, and P. Burnard on an early draft of this manuscript are appreciated. Reviews by Samuel Niedermann and an anonymous reviewer greatly improved the manuscript. This is CRPG contribution No. 1700.

Appendix A. Supplementary data

Supplementary data associated with this article can be found, in the online version, at doi:10.1016/j.epsl.2004.10.009.

References

[1] T.E. Cerling, Dating geomorphologic surfaces using cosmogenic ^{3}He, Quat. Res. 33 (1990) 148–156.

[2] M.D. Kurz, D. Colodner, T.W. Trull, R.B. Moore, K. O'Brien, Cosmic ray exposure dating with in situ produced cosmogenic ^{3}He: results from young Hawaiian lava flows, Earth Planet. Sci. Lett. 97 (1990) 117–189.

[3] S. Niedermann, Cosmic-ray-produced noble gases in terrestrial rocks: dating tools for surface processes, in: D. Porcelli, C.J. Ballentine, R. Wieler (Eds.), Noble Gases in Geochemistry and Cosmochemistry, Rev. Min. Geochem. 47 (2002) 731–784.

[4] T.E. Cerling, H. Craig, Geomorphology and in situ cosmogenic isotopes, Annu. Rev. Earth Planet. Sci. 58 (1994) 249–255.

[5] P.L. Barnard, L.A. Owen, M.C. Sharma, R.C. Finkel, Natural and human-induced landsliding in the Garhwal Himalaya of northern India, Geomorphology 40 (2001) 21–35.

[6] E.T. Brown, R.F. Stallard, M.C. Larsen, G.M. Raisbeck, F. Yiou, Denudation rates determined from the accumulation of in situ produced ^{10}Be in the Luquillo Experimental Forest, Puerto Rico, Earth Planet. Sci. Lett. 129 (1995) 193–202.

[7] D.E. Granger, C.S. Riebe, J.W. Kirchner, R.C. Finkel, Modulation of erosion on steep granitic slopes by boulder armoring, as revealed by cosmogenic ^{26}Al and ^{10}Be, Earth Planet. Sci. Lett. 186 (2001) 269–281.

[8] D. Vance, M. Bickle, S. Ivy-Ochs, P.W. Kubik, Erosion and exhumation in the Himalaya from cosmogenic isotope inventories of river sediments, Earth Planet. Sci. Lett. 206 (2002) 273–288.

[9] K. Nishiizumi, E.L. Winterer, C.P. Kohl, J. Klein, R. Middleton, D. Lal, J.R. Arnold, Cosmic ray production rates of ^{10}Be and ^{26}Al in quartz from glacially polished rocks, J. Geophys. Res. 94 (1989) 17907–17915.

[10] P.W. Kubik, S. Ivy-Ochs, J. Masarik, M. Frank, C. Schlüchter, ^{10}Be and ^{26}Al production rates deduced from an instantaneous event within the dendro-calibration curve, the landslide of Köfels, Ötz Valley, Austria, Earth Planet. Sci. Lett. 161 (1998) 231–241.

[11] J. Leland, M.R. Reid, D.W. Burbank, R. Finkel, M. Caffee, Incision and 19 differential bedrock uplift along the Indus River near Nanga Parbat, Pakistan Himalaya, from ^{10}Be and ^{26}Al exposure age dating of bedrock straths, Earth Planet. Sci. Lett. 154 (1998) 93–107.

[12] J.M. Schäfer, S. Ivy-Ochs, R. Wieler, I. Leya, H. Baur, G.H. Denton, C. Schlüchter, Cosmogenic noble gas studies in the oldest landscape on Earth: surface exposure age of the dry valleys, Antarctica, Earth Planet. Sci. Lett. 167 (1999) 215–226.

[13] M.D. Kurz, In situ production of terrestrial cosmogenic helium and some applications to geochronology, Geochim. Cosmochim. Acta 50 (1986) 2855–2862.

[14] J.M. Licciardi, M.D. Kurz, P.U. Clark, E.J. Brook, Calibration of cosmogenic ^{3}He production rate of Holocene lava flows in Oregon, USA, and effects of the Earth's magnetic field, Earth Planet. Sci. Lett. 172 (1999) 261–271.

[15] E.J. Brook, M.D. Kurz, R.P. Ackert, G.H. Denton, E.T. Brown, G.M. Raisbeck, F. Yiou, Chronology of Taylor Glacier advances in Arena Valley, Antarctica, using in situ cosmogenic ^{3}He and ^{10}Be, Quat. Res. 39 (1993) 11–23.

[16] T.W. Trull, M.D. Kurz, J. Jenkins, Diffusion of cosmogenic ^{3}He in olivine and quartz. implication for surface exposure dating, Earth Planet. Sci. Lett. 103 (1991) 241–256.

[17] K.A. Farley, Helium diffusion from apatite; general behavior as illustrated by Durango fluorapatite, J. Geophys. Res. 105 (2000) 2903–2914.

[18] R.A. Wolf, K.A. Farley, D.M. Kass, Modeling of the temperature sensitivity of the apatite (U–Th)/He thermochronometer, Chem. Geol. 148 (1998) 105–114.

[19] T.J. Dunai, K. Roselieb, Sorption and diffusion of helium in garnet: implication for volatile tracing and dating, Earth Planet. Sci. Lett. 139 (1996) 411–421.

[20] T.E. Cerling, H. Craig, Cosmogenic ^{3}He production rates from 39N to 46N lat., western USA and France, Geochim. Cosmochim. Acta 58 (1994) 249–255.

[21] T.J. Dunai, J.R. Wijbrans, Long-term cosmogenic ^{3}He production rates (152 ka–1.35 Ma) from ^{40}Ar/^{39}Ar dated basalt flows at 29N lat., Earth Planet. Sci. Lett. 176 (2000) 147–156.

[22] R.P. Ackert, B.S. Singer, H. Guillou, M.R. Kaplan, M.D. Kurz, Long-term cosmogenic ^{3}He production rates from ^{40}Ar/^{39}Ar and K–Ar dated Patagonian lava flows at 47°S, Earth Planet. Sci. Lett. 210 (2003) 119–1136.

[23] T. Staudacher, C.J. Allègre, Ages of the second caldera of Piton de la Fournaise volcano (Réunion) determined by cosmic ray produced ^{3}He and ^{21}Ne, Earth Planet. Sci. Lett. 119 (1993) 395–404.

[24] P. Sarda, T. Staudacher, C.J. Allègre, A. Lecomte, Cosmogenic neon and helium at Réunion: measurement of erosion rate, Earth Planet. Sci. Lett. 119 (1993) 405–417.

[25] J.M. Licciardi, P.U. Clark, E.J. Brook, K.L. Pierce, M.D. Kurz, D. Elmore, P. Sharma, Cosmogenic ^{3}He and ^{10}Be chronologies of the late Pinedale northern Yellowstone ice cap, Montana, USA, Geology 29 (2001) 1095–1098.

[26] S.G. Wells, L.D. McFadden, J. Poths, C.T. Olinger, Cosmogenic ^{3}He surface exposure dating of stone pavements: implications for landscape evolution in deserts, Geology 23 (1995) 613–616.

[27] T.E. Cerling, R.H. Webb, R.J. Poreda, A.D. Rigby, T.S. Melis, Cosmogenic ^{3}He ages and frequency of late Holocene debris flows from Prospect Canyon, Grand Canyon, USA, Geomorphology 27 (1999) 93–111.

[28] A. Pêcher, Déformation et métamorphisme associés à une zone de cisaillement: Exemple du grand chevauchement central himalayen (M.C.T), transversale des Annapurnas et du Manaslu Népal, PhD thesis, Université Scientifique et Médicale de Grenoble, 1978, 353 pp.

[29] M. Colchen, P.L. Fort, A. Pêcher, Notice explicative de la carte géologique Annapurna-Manaslu-Ganesh (Himalaya du Népal) au 1:200000e, Ed. Cent. Natl. Rech. Sci. (1986).

[30] P. Copeland, The When and Where of the Growth of the Himalaya and Tibetan Plateau, in: W.F. Ruddiman (Ed.), Tectonic uplift and climate change, 1997, pp. 19–40.

[31] A. Pêcher, The contact between the Higher Himalayan Crystallines and the Tibetan Sedimentary Series: Miocene large scale dextral shearing, Tectonics 10 (1991) 587–598.

[32] R. Braucher, Utilisation du ^{10}Be cosmogénique produit in-situ pour l'étude de la dynamique des latérites en zone intertropicale, PhD thesis, Université de Aix-Marseille III, 1998, 112 pp.

[33] E.T. Brown, J.M. Edmond, J.M. Raisbeck, M.D. Kurz, F. Yiou, E.J. Brook, Examination of surface exposure ages of Antarctic moraines using in situ produced ^{10}Be and ^{26}Al, Geochim. Cosmochim. Acta 55 (1991) 2269–2283.

[34] D.L. Bourlès, Etude de la géochimie de l'isotope cosmogénique ^{10}Be et de son isotope stable ^{9}Be en milieu océanique. Application à la datation des sédiments marins, PhD thesis, Paris-Sud Centre d'Orsay, 1988, 227 pp.

[35] E.T. Brown, J.M. Edmont, G.M. Raisbeck, D.L. Bourlès, F. Yiou, C.I. Measures, Beryllium isotope geochemistry in tropical river basins, Geochim. Cosmochim. Acta 56 (1992) 1607–1624.

[36] G.M. Raisbeck, The AMS facility at Gif-sur-Yvette: progress, perturbations and projects, Nucl. Instrum. Methods Phys. Res. B 92 (1994) 43–46.
[37] F. Humbert, Solubilité de l'azote dans les silicates liquides, PhD thesis, Université Henri Poincaré-Nancy 1, 1998, 233 pp.
[38] B. Marty, F. Humbert, Nitrogen and argon isotopes in oceanic basalts, Earth Planet. Sci. Lett. 152 (1997) 101–112.
[39] B. Marty, M. Lenoble, N. Vassard, Nitrogen, helium and argon in basalt: a static mass spectrometry study, Chem. Geol. 120 (1995) 183–195.
[40] B. Marty, R. Pik, Y. Gezahegn, Helium isotopic variations in Ethiopian plume lavas: nature of magmatic sources and limit on lower mantle contribution, Earth Planet. Sci. Lett. 144 (1996) 223–237.
[41] R. Zito, D.J. Donahue, S.N. Davis, H.W. Bentley, P. Fritz, Possible sub-surface production of ^{14}C, Geophys. Res. Lett. 1 (1980) 235–238.
[42] J.N. Andrews, The isotopic composition of radiogenic helium and its use to study groundwater movement in confined aquifers, Chem. Geol. 49 (1985) 339–351.
[43] J. Carignan, P. Hild, G. Mevelle, J. Morel, D. Yeghicheyan, Routine analyses of trace element in geological samples using flow injection and low pressure on-line liquid chromatography coupled to ICP-MS: a study of geochemical reference materials BR, DR-N, UB-N, AN-G and GH, Geostand. Newsl. 25 (2001) 187–198.
[44] J.O. Stone, Air pressure and cosmogenic isotope production, J. Geophys. Res. 105 (B10) (2000) 23753–23759.
[45] R.J. Poreda, T.E. Cerling, Cosmogenic neon in recent lavas from the western United States, Geophys. Res. Lett. 19 (1992) 1863–1866.
[46] J. Masarik, Numerical simulation of in-situ production of cosmogenic nuclides, Geochim. Cosmochim. Acta Goldschmidt Conf. Abstr. 2002 (2002) 491.
[47] J. Masarik, R.C. Reedy, Terrestrial cosmogenic-nuclide production systematics calculated from numerical simulations, Earth Planet. Sci. Lett. 136 (1995) 381–395.
[48] D. Lal, Cosmic ray labeling of erosion surfaces: in situ nuclide production rates and erosion models, Earth Planet. Sci. Lett. 104 (1991) 424–439.
[49] T.J. Dunai, Scaling factors for production rates of in situ produced cosmogenic nuclides: a critical reevaluation, Earth Planet. Sci. Lett. 176 (2000) 157–169.
[50] A.W. Laughlin, J. Poths, H.A. Healey, S. Reneau, G. WoldeGabriel, Dating of Quaternary basalt using cosmogenic ^{3}He and ^{14}C methods with implications for excess ^{40}Ar, Geology 22 (1994) 135–138.
[51] J.C. Gosse, F.M. Phillips, Terrestrial in situ cosmogenic nuclides: theory and application, Quat. Sci. Rev. 20 (2001).
[52] K. Nishiizumi, J. Klein, R. Middleton, H. Craig, Cosmogenic ^{10}Be, ^{26}Al, and $^{3}He_{in}$ olivine from Maui lavas, Earth Planet. Sci. Lett. 98 (1990) 263–266.
[53] D. Lal, Production of ^{3}He in terrestrial rocks, Chem. Geol. 66 (1987) 89–98.
[54] R. Michel, M. Lüpke, U. Herpers, R. Rösel, M. Suter, B. Dittrich-Hannen, P.W. Kubik, D. Filges, P. Cloth, Simulation and modelling of the interaction of galactic protons with stony meteoroids, Planet. Space Sci. 43 (3/4) (1995) 557–572.
[55] D. Lal, B. Peters, Cosmic-ray produced radioactivity on the Earth, in: K. Sitte (Ed.), Handbuch der Physik 46 (1967) 551–612.
[56] E.T. Brown, T.W. Trull, P. Jean-Baptiste, G. Raisbeck, D. Bourlès, F. Yiou, B. Marty, Determination of cosmogenic production rates of ^{10}Be, ^{3}He and ^{3}H in water, Nucl. Instrum. Methods Phys. Res. B 172 (2000) 873–883.
[57] E. Gayer, Taux d'érosion et chronologie glaciaire en Himalaya, Développement et applications de la mesure d'hélium cosmogénique dans les grenats, Institut National Polytechnique de Lorraine, 2003, 192 pp.